Should a Franck-Condon or a Curve-Crossing Picture be Applied to Ion-Target Collisional Activation? A Study of keV $CO_2^{+\cdot}$/He Collisions by Emission Spectroscopy

Clement Poon and Paul M. Mayer

Department of Chemistry, University of Ottawa, Ottawa, Ontario, Canada

Collision-induced photon emissions (CIE) were observed for keV $CO_2^{+\cdot}$/He collisions from 190 to 1020 nm. The emissions were assigned to the $\Delta\nu = 0$ band of the $CO_2^{+\cdot}$ B $^2\Sigma_u^+ \rightarrow$ X $^2\Pi_g$ electronic transition and the $\Delta\nu = +3, +2, +1, 0, -1, -2, -3$ vibrational transition progression in the $CO_2^{+\cdot}$ A $^2\Pi_u \rightarrow$ X $^2\Pi_g$ electronic transition. The other peaks arise from the emissions of excited $O^{\cdot}$ fragment atoms and the target gas. The relative intensities of the $CO_2^{+\cdot}$ and $O^{\cdot}$ emissions are independent of the ion translational energy above 3 keV, supporting the curve-crossing mechanism for collisional excitation. Investigation of the relative intensities within the A $^2\Pi_u \rightarrow$ X $^2\Pi_g$ emission of $CO_2^{+\cdot}$ indicates that the vibrational distribution is well described by the Franck-Condon principle at high collision energy, a consequence of short collision time but not necessarily an indication of vertical transitions. Below 3 keV ion translational energy, vibrational excitation in the A $^2\Pi_u$ electronic state was observed. The observation is consistent with the explanation that the reaction occurs at small impact parameters, in which short-range, repulsive interactions between the projectile and the target result in direct translational-vibrational excitation. (J Am Soc Mass Spectrom 2008, 19, 1551–1558) © 2008 American Society for Mass Spectrometry

Detection of photon emissions from collisionally-activated species provides information on the electronic states that are accessible by collisions. This type of emission spectroscopy is often carried out in a mass spectrometer for the study of ion-neutral collisions where the projectile ions collide with a neutral target gas in a collision cell [1–5].

Early experiments were carried out to acquire laboratory data on reactions that occur in the earth's atmosphere, in particular on the charge-transfer process. Consistency between experimental results with those predicted by Franck-Condon factors is often used as a sign that electronic transitions in the collision process are vertical [6–8]. Moore and Doering have studied the vibrational distribution of the N_2^+ B $^2\Sigma_u^+$ state by observing the relative band intensities of the $\Delta\nu = -1$ sequence of the B $^2\Sigma_u^+ \rightarrow$ X $^2\Sigma_g^+$ emission resulting from the charge-transfer of various projectile atomic/diatomic ions with N_2 [9]. They concluded that the observed vibrational distributions depend heavily on the laboratory velocity of the reactant ion but very little on its chemical nature. When the velocity is below 10^8 cm/s, the vibrational distributions no longer agree with those predicted by the Franck-Condon principle. This was initially explained as distortion of the target molecule electron cloud by the impinging ion at low velocities [9, 10]. This explanation, however, could not explain the similar behavior in the direct excitation process observed in $N_2^{+\cdot}$/target collisions [11]. Kelley et al. [8, 12] later explained this phenomenon with a more general qualitative curve-crossing model based on the assumption that deviations from vertical transitions during collisions are caused by a short-range, repulsive interaction between the projectile and the target and that these short-range interactions result in the direct translational-vibrational excitation in both the initial and the final electronic states of the diatomic molecule [4, 8, 12]. The fact that short-range forces are involved means that the reaction occurs at small impact parameters. As such, the diatomic molecule cannot be regarded as being isolated. In other words, distortion occurs by chemical forces that are operative in any short-range encounter between two atoms or molecules. Landau and Zener expressed the probability (P) of crossing from one potential curve to another in terms of the slope (dV/dr) difference at the crossing point and the relative velocity (v) of the two colliding species [13, 14].

$$P = e^{-2\delta} \quad \text{where} \quad \delta = \frac{(2\pi)^{3/2} H_{12}^2 \ (R)}{\left(\left| \frac{dV_1}{dr} - \frac{dV_2}{dr} \right| \right) h\nu} \tag{1}$$

where H_{12} is the off diagonal matrix element describing the transition between two electronic states (1 and 2), and h is Planck's constant.

Address reprint requests to Professor P. M. Mayer, Department of Chemistry, University of Ottawa, 10 Marie-Curie, Ottawa, Ontario K1N 6N5, Canada. E-mail: pmmayer@uottawa.ca

1044-0305/08/$32.00
doi:10.1016/j.jasms.2008.06.004

Published online June 27, 2008
Received February 28, 2008
Revised June 12, 2008
Accepted June 13, 2008

Recently, we have shown that for both keV $N_2^{+\cdot}$/He and $N_2^{+\cdot}$/Ar collisions, the relative emission intensity between the fragments and the precursor ions are independent of ion translational energy [15, 16]. According to the vertical transition model (in which excitation is assumed to be analogous to electron or photon excitation), increasing collision energy should increase emissions from species formed at higher internal energy (such as excited-state fragments). Our observation was therefore in contradiction with vertical transitions but supports the curve-crossing mechanism. If the curve-crossing mechanism is dominant, transitions occur at a few curve-crossing points and may then be followed by a complicated sequence of nonadiabatic interactions. According to the Landau-Zener curve-crossing model, higher ion velocity (i.e., higher ion translational energy) will increase the probability that the system will follow the diabatic curves, forming excited-state species. As such, the same excited-state species will be formed at all ion translational energies, and the distribution of these species will be constant.

Similarly, charge-transfer processes with CO_2 have been studied by several groups [17–22]. The $B\ ^2\Sigma_u^+ \rightarrow X\ ^2\Pi_g$ and $A\ ^2\Pi_u \rightarrow X\ ^2\Pi_g$ emissions are the dominant emissions observed in the wavelength range of 200–500 nm. At high velocity, the vibrational energy distribution in CO_2^+ (A) was found to be independent of velocity in H_2^+/CO_2 and He^+/CO_2 charge-transfer processes, whereas at velocities below 4×10^7 cm/s the relative populations of the low vibrational states increases monotonically with decreasing projectile ion velocity [17]. In the study of Ne^+/CO_2, the $B\ ^2\Sigma_u^+ \rightarrow X\ ^2\Pi_g$ and $A\ ^2\Pi_u \rightarrow X\ ^2\Pi_g$ emissions are monitored as a function of precursor ion translational energy. It was found that below 2 keV, the ratio of $B^2\Sigma_u^+ \rightarrow X\ ^2\Pi_g$ to $A\ ^2\Pi_u \rightarrow X\ ^2\Pi_g$ emissions decreases with translational energy [19].

An initial study from our laboratory on the emissions of $CO_2^{+\cdot}$/He collisions from 190 to 680 nm also showed both $B\ ^2\Sigma_u^+ \rightarrow X\ ^2\Pi_g$ and $A\ ^2\Pi_u \rightarrow X\ ^2\Pi_g$ emission bands [23]. To our knowledge, collision-induced emissions (CIE) resulting from the direct excitation of $CO_2^{+\cdot}$ precursor ions has never been observed over a range of ion translational energies. In comparison to collisions involving $N_2^{+\cdot}$, emissions from the fragments are also comparatively stronger, providing a more reliable comparison of the relative intensities at different ion translational energies. In the present article, we will present a comparison of the relative emission intensities between the fragments and the precursor ion as well as within the $A\ ^2\Pi_u \rightarrow X\ ^2\Pi_g$ emission band of $CO_2^{+\cdot}$ at different ion translational energies. The vibrational distribution of the $A\ ^2\Pi_u$ state determined from the emission band is also compared to that obtained from the electron ionization (EI) process and from photoelectron spectroscopy (PES).

Experimental

All experiments were performed on a modified VG ZAB mass spectrometer. The original, double-focusing mass spectrometer [24, 25] and the added third field-free region (3FFR) with an experimental zone designed for this work have been described previously [3, 15].

The precursor ion $CO_2^{+\cdot}$ is generated from CO_2 by electron ionization and is transmitted to the 3FFR where it collides with the target gas in the deceleration-reacceleration collision cell assembly at a collision gas pressure that reduces the pre-cell ion flux by 10% (i.e., single collision condition) [26]. A spectrograph (Acton SpectraPro 275, 27.5 focal length, 1200 g mm^{-1} holographic grating) (Acton Research Corp, Acton, Mass, USA) and a thermoelectrically-cooled charge-coupled device (CCD) detector (Andor DV401-UV, front-illuminated with UV coating, Andor Technology, Belfast, Northern Ireland) have been installed above the collision cell for the detection of photon emissions resulting from ion-target collisions. Emissions from the excited ions and the target gas were directly observed with the CCD detector cooled to a temperature of −35 °C. The time window of observation ranges from 0.00–0.06 μs for 8 keV $CO_2^{+\cdot}$ to 0.00–0.12 μs for 2 keV $CO_2^{+\cdot}$, depending on the ion translational energy. The entrance slit of the spectrograph is set to 3.0 mm to maximize emission signal intensity. This resulted in a spectral resolution of 8.5 nm (measured at full width at half-height for atomic lines). Optical emissions were recorded from 190 to 1020 nm using the Andor MCD 2.63.1.8 program and were recorded in 14 separate segments, each being 50 to 70 nm wide. Two accumulations of 15 min were collected at 8 keV ion translational energy for each segment at full vertical binning reading mode. CIE spectrum of lower projectile ion translational energy (from 7 to 2 keV) were collected for the wavelength range 190–536 nm and 768–875 nm sections that contain the emissions from $CO_2^{+\cdot}$ and its fragments. Total acquisition time for each of the separate segments ranges from 1 to 5 h. Each segment was background subtracted and background spectra were collected before signal acquisition with exactly the same conditions except without an ion beam. Spectral spikes resulting from cosmic rays were removed digitally by the program. Horizontal binning was performed manually in the ASCII file by combining data of every 20 pixel columns and the overlapping portion of the spectrum at the two ends of each window was averaged. All ion translational energies were obtained by varying the source accelerating voltage, except at 2 keV, which was obtained from a 3 keV ion beam with +1 kV voltage applied to the collision cell assembly to decelerate the ions.

A higher-resolution spectrum (262–442 nm) was obtained by reducing the entrance slit width to 1.0 mm, resulting in a spectral resolution of 3.0 nm, and the data acquisition time of each segment was increased to 5 h.

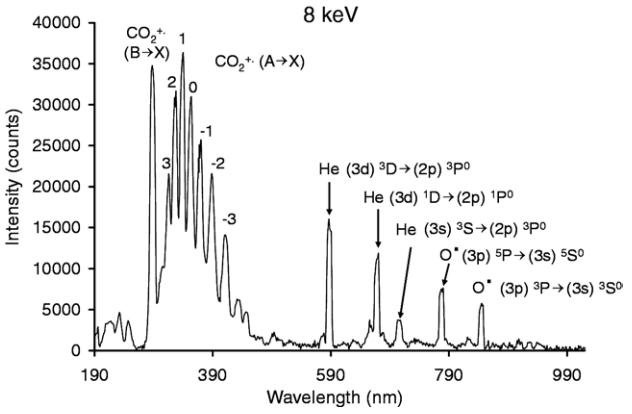

Figure 1. Collision-induced emission spectrum (190–1020 nm) of $CO_2^{+\cdot}$/He collisions at 8 keV projectile ion translational energy. Collision gas pressure corresponded to 90% ion beam transmission (total data acquisition time per section: 30 min).

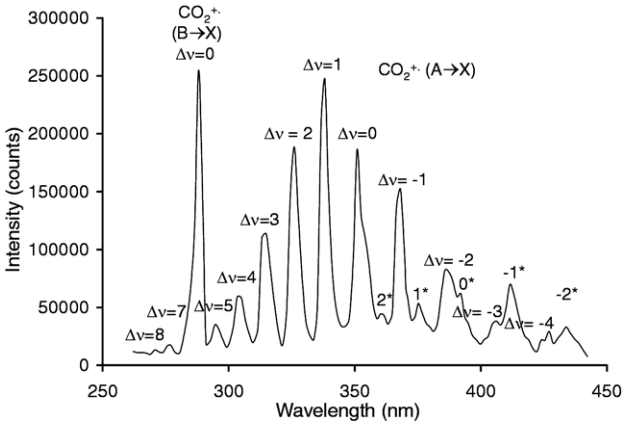

Figure 2. Collision-induced emission spectrum (262–442 nm) of 8 keV $CO_2^{+\cdot}$/He collisions obtained with an entrance slit width of 1.0 mm (total data acquisition time per section: 10 h).

With 80 to 90 eV electrons, ionization of CO_2 could result in $CO_2^{+\cdot}$ being formed in excited electronic states. However, the radiative lifetimes of the A $^2\Pi_u$ and B $^2\Sigma_u^+$ states of $CO_2^{+\cdot}$ are 116 and 145 ns, respectively [27, 28]. When compared with the time required for the ions to reach the collision chamber, which ranges from 17 to 34 μs depending on the accelerating voltage, virtually all ions that are formed initially in the A $^2\Pi_u$ or B $^2\Sigma_u^+$ state would have returned to the ground state by the time they collide with the target gas.

Results and Discussion

Emission Spectrum of $CO_2^{+\cdot}$/He Collisions

The emission spectrum over the wavelength range 190–1020 nm was obtained from $CO_2^{+\cdot}$/He collisions at 8 keV ion translational energy (Figure 1). A summary of the peak and transition assignments is presented in Table 1, Two prominent features are observed in the low wavelength region. They correspond to the $\Delta\nu = 0$ band of the $CO_2^{+\cdot}$ B $^2\Sigma_u^+ \rightarrow$ X $^2\Pi_g$ electronic transition and the $\Delta\nu = +3, +2, +1, 0, -1, -2, -3$ vibrational

Table 1. Observed emissions in Figures 1, 2, and 5, and their corresponding radiative lifetimes

Transition[a]			τ (ns)[b]	λ (nm)	Ref.
$CO_2^{+\cdot}$	B $^2\Sigma_u^+ \rightarrow$ X $^2\Pi_g$	(n,0,0)→(n,0,0) ($\Delta\nu = 0$)	~145	288	[27–29]
	A $^2\Pi_u \rightarrow$ X $^2\Pi_g$	(n,0,0)→(n−8,0,0) ($\Delta\nu = 8$)	~120	271	[27, 28, 30–33, 38]
		(n,0,0)→(n−7,0,0) ($\Delta\nu = 7$)		277	
		(n,0,0)→(n−6,0,0) ($\Delta\nu = 6$)		285	
		(n,0,0)→(n−5,0,0) ($\Delta\nu = 5$)		294	
		(n,0,0)→(n−4,0,0) ($\Delta\nu = 4$)		304	
		(n,0,0)→(n−3,0,0) ($\Delta\nu = 3$)		315	
		(n,0,0)→(n−2,0,0) ($\Delta\nu = 2$)		326	
		(n,0,0)→(n−1,0,0) ($\Delta\nu = 1$)		338	
		(n,0,0)→(n,0,0) ($\Delta\nu = 0$)		351	
		(n,0,0)→(n+1,0,0) ($\Delta\nu = -1$)		368	
		(n,0,0)→(n+2,0,0) ($\Delta\nu = -2$)		386	
		(n,0,0)→(n+3,0,0) ($\Delta\nu = -3$)		405	
		(n,0,0)→(n+4,0,0) ($\Delta\nu = -4$)		427	
		where n = 0, 1, 2, ...			
		(n,0,0)→(n−2,0,2) ($\Delta\nu = 2$)*	—	361	[21, 31–33]
		(n,0,0)→(n−1,0,2) ($\Delta\nu = 1$)*		375	
		(n,0,0)→(n,0,2) ($\Delta\nu = 0$)*		392	
		(n,0,0)→(n+1,0,2) ($\Delta\nu = -1$)*		411	
		(n,0,0)→(n+2,0,2) ($\Delta\nu = -2$)*		434	
		where n = 0, 1, 2, ...			
O·	(3p) $^5P \rightarrow$ (3s) $^5S^0$		27	779	[39, 40]
	(3p) $^3P \rightarrow$ (3s) $^3S^0$		31	845	
He	(3d) $^3D \rightarrow$ (2p) $^3P^0$		14	587	[39, 40]
	(3d) $^1D \rightarrow$ (2p) $^1P^0$		16	669	
	(3s) $^3S \rightarrow$ (2p) $^3P^0$		65	707	

[a] Transition written in notation (ν_1, ν_2, ν_3). For $CO_2^{+\cdot}$, ν_1 = symmetric stretch, ν_2 = bending mode, and ν_3 = asymmetric stretch.
[b] Lifetimes from references [27, 28, 39].

transition progression in the $CO_2^{+\cdot}$ A $^2\Pi_u \rightarrow$ X $^2\Pi_g$ electronic transition. The other peaks arise from the emissions of the excited O· fragment and the target gas, He. The single sharp peak for the B $^2\Sigma_u^+ \rightarrow$ X $^2\Pi_g$ transitions and the broad vibrational progression in the A $^2\Pi_u \rightarrow$ X $^2\Pi_g$ transition indicate a similar geometry between the B $^2\Sigma_u^+$ and the ground electronic state while that for the A $^2\Pi_u$ electronic state is substantially different, consistent with previous experimental results by fluorescence and photoelectron spectroscopy [29–33]. The X $^2\Pi_g$, A $^2\Pi_u$, and B $^2\Sigma_u^+$ states of $CO_2^{+\cdot}$ all have linear and symmetric geometries, with CO bond lengths of 1.1768, 1.2274, and 1.1805 Å, respectively [29, 30].

Vibrational Population in the A $^2\Pi_u$ State

Figure 2 presents the emission spectrum (262–442 nm) obtained at higher resolution (with an entrance slit width reduced to 1.0 mm). The vibrational progression in the A $^2\Pi_u \rightarrow$ X $^2\Pi_g$ transition is better resolved, including several peaks at low wavelength corresponding to the $\Delta\nu$ = 5, 7, and 8 of the A $^2\Pi_u \rightarrow$ X $^2\Pi_g$ transition. The peak for the $\Delta\nu$ = 6 transition likely overlaps with the B $^2\Sigma_u^+ \rightarrow$ X $^2\Pi_g$ emission, giving rise to the tailing on one side of the peak. In addition, another vibrational progression marked by asterisks was observed. The assignment of this series is also included in Table 1.

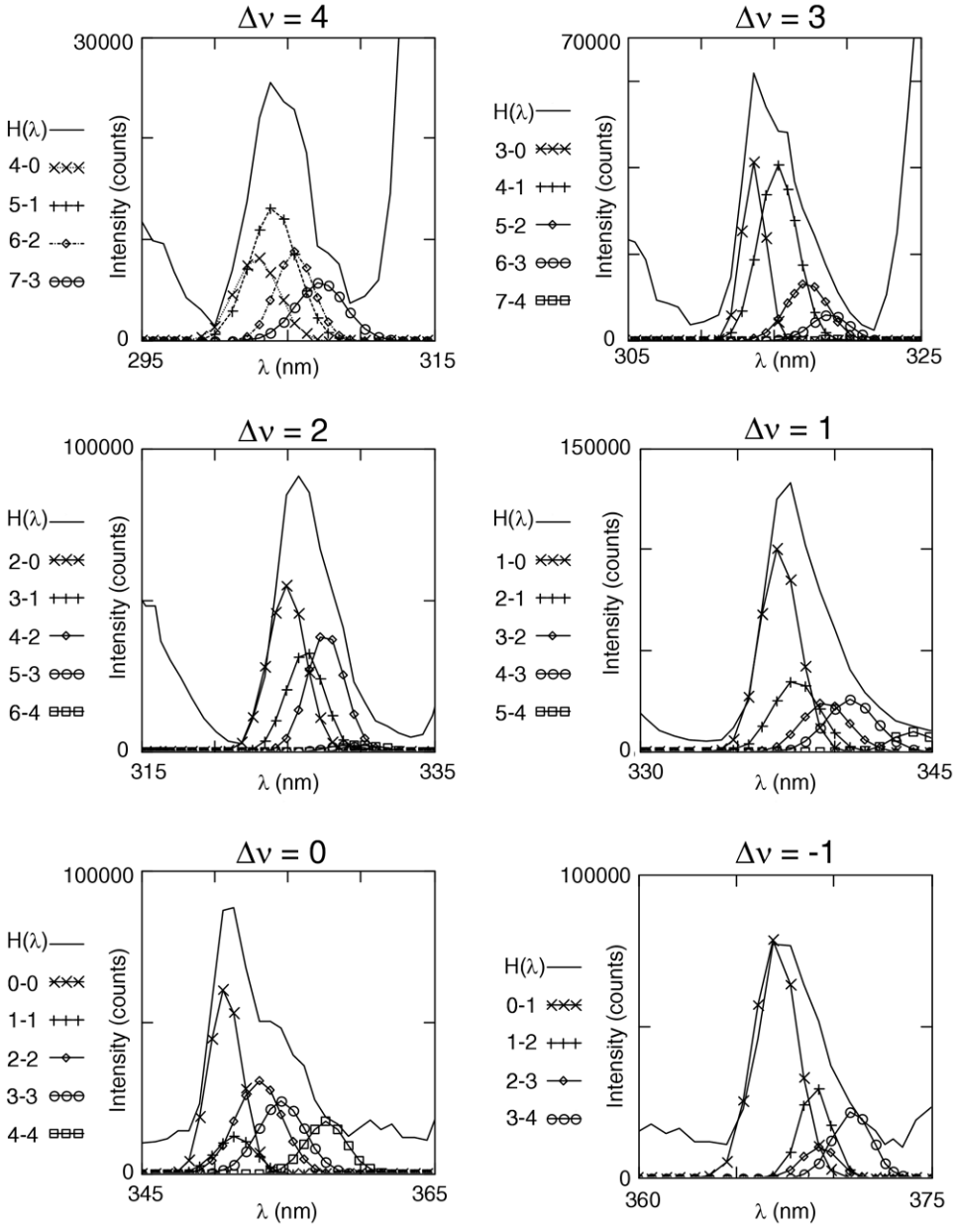

Figure 3. Peaks of the A $^2\Pi_u \rightarrow$ X $^2\Pi_g$ emission of $CO_2^{+\cdot}$ in the CIE spectrum fitted with Gaussian functions representing transitions between different vibrational states in the ground and the excited-state. The experimental data is shown as H(λ) and individual vibrational transitions from (i,0,0) of the A $^2\Pi_u$ state to (j,0,0) of the X $^2\Pi_g$ state are listed as i–j.

Table 2. Relative vibrational populations of the $CO_2^{+\cdot}$ ($A\ ^2\Pi_u$) state

Method	Electron energy (eV)	Vibrational level (i, 0, 0) 0	1	2	3	4	5	6	7	Ref.
CIE		17	12	15	18	19	9	5	4	This work
EI	30	12	26	21	19	13	6	2	1	[36]
	50	13	23	22	20	13	6	2	1	
	100	13	23	21	19	14	6	2	1	
	300	14	23	23	20	14	5	2	1	
PES		8	18	28	18	12	9	4	2	[36, 41]

Figure 2 was used to estimate the vibrational distribution of the $A\ ^2\Pi_u$ state of $CO_2^{+\cdot}$ after collisions. Each peak in the CIE spectrum is composed of several individual components corresponding to transitions between different vibrational states. For example, the peak of $\Delta\nu = 0$ contains contribution from transitions 0-0, 1-1, 2-2 etc. We therefore used a number of Gaussian functions and the Franck-Condon factors between the $A\ ^2\Pi_u$ and $X\ ^2\Pi_g$ state of $CO_2^{+\cdot}$ from McCallum and Nicholls [34] to fit for the vibrational population [from (0, 0, 0) to (7, 0, 0)]. The emission intensity ($I_{em}^{v'v''}$) can be expressed as [35]

$$I_{em.}^{\nu'\nu''} = K\frac{N_{\nu'}}{(\lambda_{\nu',\nu''})^4}\bar{R}_e^2 q_{\nu',\nu''}$$

where $N_{v'}$ is the population of the v′ vibrational level, $q_{v',v''}$ and $\lambda_{v',v''}$ are the Franck-Condon factor and the wavelength, respectively, for the v′-v″ band. $\bar{R}_e^2$ is the average electronic transition moment for the transition and K is a constant. Within a sequence, $\bar{R}_e$ is nearly constant. Therefore, for each peak in the emission band, we can express the fitting approach in the generic form as shown below:

$$H(\lambda) = \frac{N_i}{(\lambda_{ij})^4}\cdot\frac{q_{ij}}{q_{tot}}\cdot G(\lambda) + \frac{N_{i+1}}{(\lambda_{i+1\,j+1})^4}\cdot\frac{q_{i+1\,j+1}}{q_{tot}}\cdot G(\lambda) + \frac{N_{i+2}}{(\lambda_{i+2\,j+2})^4}\cdot\frac{q_{i+2\,j+2}}{q_{tot}}\cdot G(\lambda) + \ldots$$

H(λ) represents the peak to be fitted by a number of smaller Gaussian functions G(λ), each of them scaled by the population N of the emitting vibrational state and the Franck-Condon factor $q_{i,j}$ between vibrational states (i,0,0) of the $A\ ^2\Pi_u$ state and (j,0,0) of the $X\ ^2\Pi_g$ state; q_{tot} is the sum of the Franck-Condon factors used and $\lambda_{i,j}$ is the wavelength of the emission. The constant K is taken into account in the Gaussian function G(λ). Figure 3 shows the result of the fits. The relative vibrational populations for states (0, 0, 0) to (7, 0, 0) are listed in Table 2. Our results are generally similar to those produced by electron impact on jet-cooled CO_2 and photoelectron spectroscopy [36].

To determine if the differences in these populations cause any dramatic differences in the resulting emission spectrum, spectra (330–370 nm) were synthesized from the vibrational distributions obtained from the three methods (Figure 4). All three spectra exhibit similar vibrational patterns; however, the relative intensity of the $\Delta\nu = 0$ and -1 bands appears to be higher for CIE than for PES. The small difference appears to be due to a larger population in the ground vibrational state obtained from the CIE results and could be a result of intramolecular vibrational redistribution (IVR) before emission. The vibrational distribution in the $A\ ^2\Pi_u$ state as a result of collisions therefore resembles those predicted by the Franck-Condon factors, an indication that for 8 keV $CO_2^{+\cdot}$/He collisions, the collision time is indeed short enough in comparison to the vibrational period that the Franck-Condon principle can be applied to predict the relative intensity of an emission band resulting from collisional activation.

Relative Intensities as a Function of Ion Translational Energy

The emission spectra over the wavelength ranges 190–536 nm and 768–875 nm from 7 keV to 2 keV ion translational energy are presented in Figure 5. These are

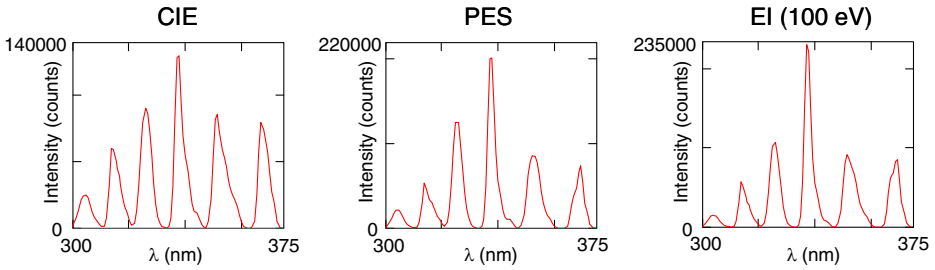

Figure 4. Relative intensities of the $CO_2^{+\cdot}$ $A\ ^2\Pi_u \rightarrow X\ ^2\Pi_g$ emission that would be expected using the vibrational distribution from CIE, PES and EI (at 100 eV electron energy).

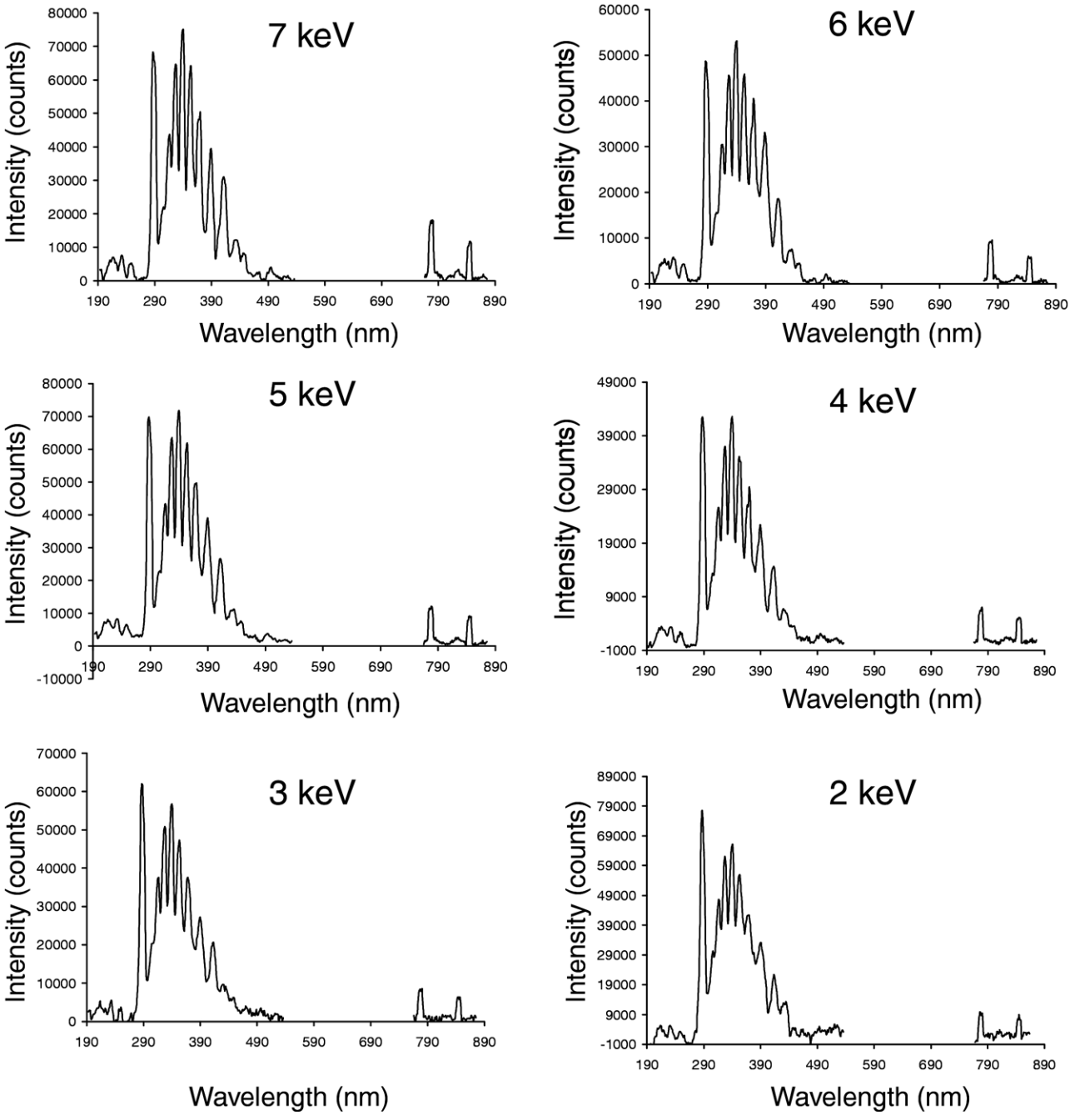

Figure 5. CIE spectra (190–536 nm and 768–875 nm) of $CO_2^{+\cdot}$/He collisions at various projectile ion translational energies. Collision gas pressure corresponds to 90% ion beam transmission [total data acquisition time per section: 1 h (7 keV to 4 keV), 3 h (3 keV), and 5 h (2 keV)].

the sections that contain emissions from the precursor ion $CO_2^{+\cdot}$ and its fragments whose relative intensities are of interest to us in the study. The intensities of the emissions from the target gas cannot be directly compared with those from the projectile ions or the fragments since the spatial distribution of collisions across the collision cell is unknown. The relative emission intensities of $CO_2^{+\cdot}$ and $O^{\cdot}$ at various collision energies are presented in Figure 6 and Table 3. The intensities have been corrected for the difference in radiative lifetime as only a portion of the emission from the excited-state species were detected. The correction was performed based on our previous conclusion that the majority of collision events take place under the window [15]. Two additional plots (one with no lifetime correction and one with a different lifetime correction) are also included in the supporting document (Supplementary Figure 1, which can be found in the electronic version of this article). Comparison of these plots results in a similar conclusion regarding the location of colli-

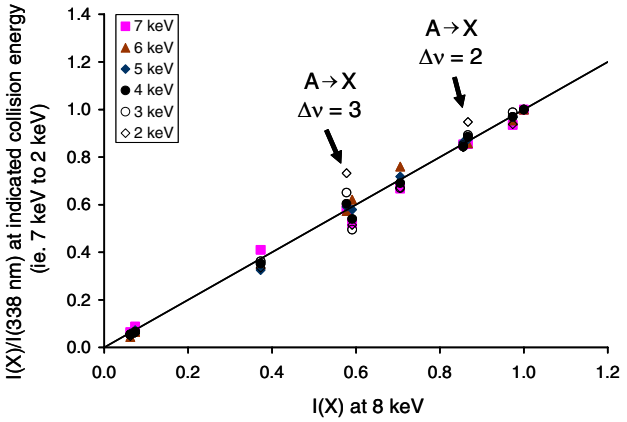

Figure 6. Lifetime-corrected plot of the relative emission intensities of $CO_2^{+\cdot}$ and $O^{\cdot}$ at various ion translational energies versus those at 8 keV. I(X) represents the intensity of $CO_2^{+\cdot}$ and $O^{\cdot}$ and I(338 nm) the intensity of $\Delta\nu = 1$ of the A $^2\Pi_u \rightarrow$ X $^2\Pi_g$ transition of $CO_2^{+\cdot}$.

sions being under the observation window for the current study.

A good correlation can be observed in Figure 6 between most points and the y = x line. The fact that most points fall along the y = x line indicate that these relative intensities do not change with ion translational energy, in agreement with the curve-crossing mechanism for collisional activation. Two points result in larger deviations from the line. They correspond to $\Delta\nu = 3$ and $\Delta\nu = 2$ of the $CO_2^{+\cdot}$ A $^2\Pi_u \rightarrow$ X $^2\Pi_g$ emission. This is interpreted as the growing importance of vibrational excitation in addition to electronic excitation at lower ion translational energy. Based on the collision cross section of CO_2 [37], the interaction time between $CO_2^{+\cdot}$ and He is estimated to be near 10^{-14} s at 2 keV ion translational energy, bringing it close to the vibrational period of about 2×10^{-14} s. At these ion translational energies, the collision time is no longer much shorter than the time of a vibrational period. Therefore, the Franck-Condon principle no longer holds. The increase in vibrational excitation with decreasing ion translational energy is opposite of what was observed in the charge-transfer process with CO_2 [17] but is consistent with the direct excitation process involving $N_2^{+\cdot}$ precursor ions [9–12]. Kelley et al. [4, 8, 12] proposed that the reaction occurs at small impact parameters in which short-range, repulsive interaction between the projectile and the target result in direct translational-vibrational excitation.

The B $^2\Sigma_u^+ \rightarrow$ X $^2\Pi_g$ emission appears to increase with respect to the A $^2\Pi_u \rightarrow$ X $^2\Pi_g$ ($\Delta\nu = 1$) emission in the 3 and 2 keV CIE spectra. This is primarily due to vibrational excitation in the A $^2\Pi_u$ state as the peak for the B $^2\Sigma_u^+ \rightarrow$ X $^2\Pi_g$ emission overlaps with several peaks from the broad vibrational progression of the A $^2\Pi_u \rightarrow$ X $^2\Pi_g$ transition ($\Delta\nu = 5$, 6 and 7) (see Figures 1 and 5). Corrections were made to deconvolute the two components, resulting in consistent relative intensities for the B $^2\Sigma_u^+ \rightarrow$ X $^2\Pi_g$ emission as a function of ion translational energy (Table 3).

Conclusions

While the mechanism for photo-excitation is widely accepted as a result of vertical transitions, that for collisional excitation is often divided between vertical transitions and curve crossings, especially for small molecules and ions. Based on the short collision time involved in keV collisions, a number of authors often immediately invoke the Franck-Condon principle. Several studies on the relative intensities within an emission band have confirmed the Franck-Condon picture. In our experiments, we monitored the population distribution of the excited states by observing emissions from the precursor ions and its fragments. While our investigation of the relative intensities within the A $^2\Pi_u \rightarrow$ X $^2\Pi_g$ emission band of $CO_2^{+\cdot}$ demonstrates similar Franck-Condon behavior above 3 keV ion translational energy, the fact that the relative intensities between the fragments and the precursor ions remain constant with respect to ion translational energy in keV $CO_2^{+\cdot}$/He collisions cannot be accounted for by vertical transitions. The Franck-Condon principle, which is purely based on the grounds of short transition time, can also be applied to the curve-crossing model. Therefore, linking the Franck-Condon principle immediately to vertical transitions for collisional excitation could be misleading.

Below 3 keV ion translational energy, deviation from the Franck-Condon picture started to occur for the relative intensities of the $CO_2^{+\cdot}$ emission bands. This is

Table 3. Relative emission band intensities after lifetime correction[a]

Ion translational energy (keV)	$CO_2^{+\cdot}$ B→X[b]	$CO_2^{+\cdot}$ A→X						$O^{\cdot}$	
	288 nm	315 nm	326 nm	338 nm	351 nm	368 nm	386 nm	779 nm	845 nm
8	0.97	0.58	0.87	1.00	0.86	0.71	0.59	0.37	0.07
7	0.94	0.58	0.85	1.00	0.85	0.67	0.52	0.41	0.09
6	0.95	0.57	0.86	1.00	0.86	0.76	0.62	0.35	0.07
5	0.97	0.59	0.88	1.00	0.86	0.72	0.58	0.33	0.07
4	0.97	0.60	0.89	1.00	0.84	0.69	0.54	0.35	0.07
3	0.99	0.65	0.89	1.00	0.85	0.67	0.50	0.36	0.06
2	0.94	0.73	0.95	1.00	0.84	0.67	0.51	0.33	0.06

[a] Lifetime corrections were performed by treating all collisions occurring when the ions enter the observation region.
[b] Relative intensity has been corrected by subtracting the overlapping contribution from the A→X emission (see text).

an indication that the Franck-Condon principle starts to break down as the collision time becomes comparable to the vibrational period of $CO_2^{+\cdot}$ at this ion translational energy. The gradual increase of the relative intensities at lower wavelengths of the $CO_2^{+\cdot}$ A $^2\Pi_u \rightarrow$ X $^2\Pi_g$ emission therefore indicates the growing importance of vibrational excitation at lower ion translational energy. This is consistent with the explanation that deviations from vertical transitions during collisions are caused by short-range, repulsive interactions between the projectile and the target. We therefore believe that while the Franck-Condon principle and the Franck-Condon factors can still be applied to predict the relative intensities of an emission band at high ion translational energy, the vertical transition model could be superficial and misleading for understanding collisional activation. Alternatively, the curve-crossing mechanism may be a better model for understanding keV ion-target collisions even when smaller ions such as $CO_2^{+\cdot}$ are involved.

Acknowledgments

The authors thank the Natural Sciences and Engineering Research Council (NSERC) of Canada for continuing financial support. CP thanks NSERC for a postgraduate scholarship during the tenure of which this work is completed.

References

1. Birely, J. H. Formation of N_2^+ $B^2\Sigma_u^+$ and N_2 C $^3\Pi_u$ in Collisions of H^+ and H with N_2. *Phys. Rev. A* **1974,** *10*, 550–562.
2. Doering, J. P. Cross Sections for some N_2^+ and N II Emissions Excited by 1- to 10-keV N_2^+ on N_2. *Phys. Rev.* **1964,** *133*, A1537–A1545.
3. Holmes, J. L.; Mayer, P. M.; Mommers, A. A. Photon Emissions from $N_2^{+\cdot}$ Ion Beam-Target Gas Collisions in a Modified Commercial Sector Mass Spectrometer. *Int. J. Mass Spectrom. Ion Processes* **1994,** *135*, 213–228.
4. Leventhal, J. J. The Emission of Light from Excited Products of Charge Exchange Reactions. In *Gas Phase Ion Chemistry*, Vol. III., Bowers, M. T., Ed.; Academic Press: Orlando, 1984.
5. Glenewinkel-Meyer, T.; Ottinger, C. Vibrational-State Selective Cross Sections for the Charge Transfer $H^+ + HCl(X) -> H(^2\Sigma_g) + HCl^+(A)$. *J. Chem. Phys.* **1991,** *95*, 8962–8969.
6. Bearman, G. H.; Earl, J. D.; Pieper, R. J.; Harris, H. H.; Leventhal, J. J. Ionic Excitation in Low-Energy Charge-Transfer Collisions Between He_2^+ and some Diatomic Molecules. *Phys. Rev. A* **1976,** *13*, 1734–1742.
7. Bearman, G. H.; Leventhal, J. J. Excited-State Production in Collisions of H and He with N_2, CO, and O_2 over the Energy Range 150–2400 eV. *Phys. Rev. A* **1978,** *17*, 80–89.
8. Kelley, J. D.; Bearman, G. H.; Harris, H. H.; Leventhal, J. J. Dynamic Model for Vibrionic Excitation in Low Energy Atom–Molecule Collisions. *Chem. Phys. Lett.* **1977,** *50*, 295–300.
9. Moore, J. H.; Doering, J. P. Vibrational Excitation in Ion–Molecule Collisions: H^+, H_2^+, He^+, N^+, Ne^+, and Electrons on N_2. *Phys. Rev.* **1969,** *177*, 218–223.
10. Lipeles, M. Simple Model for Vibrational Transfer in Ion–Molecule Charge Exchange Excitation. *J. Chem. Phys.* **1969,** *51*, 1252–1253.
11. Bregman-Reisler, H.; Doering, J. P. Excitation of N_2^+ Ions by Collisions with Rare-Gas Atoms. *Phys. Rev. A* **1974,** *9*, 1152–1160.
12. Kelley, J. D.; Bearman, G. H.; Harris, H. H.; Leventhal, J. J. Energy Transfer in Atom–Diatom Collisions: Vibrionic Excitation. *J. Chem. Phys.* **1978,** *68*, 3345–3351.
13. Massey, H. S. W.; Burhop, E. H. S.; Gilbody, H. B. *Electronic and Ionic Impact Phenomena*; Clarendon Press: Oxford, 1974; p. 1917.
14. Nikitin, E. E. *Theory of Elementary Atomic and Molecular Processes in Gases*; Clarendon Press: Oxford, 1974; p. 107.
15. Poon, C.; Mayer, P. M. Experimental Evidence for the Curve Crossing Mechanism for Collisional Excitation in keV $N_2^{+\cdot}$/He Collisions by Emission Spectroscopy. *J. Phys. Chem. A* **2007,** *111*, 777–782.
16. Poon, C.; Lin, Y.; Mayer, P. M. Comparison of keV $N_2^{+\cdot}$/He and $N_2^{+\cdot}$/Ar Collisions by Emission Spectroscopy and Theory. *J. Phys. Chem. A*, in press.
17. Bregman-Reisler, H.; Doering, J. P. Vibrational Energy Distribution in CO_2^+ ($A^2\Pi_u$) Ions Produced by Collisions of H_2^+ and He^+ Ions with CO_2. *Chem. Phys. Lett.* **1974,** *27*, 199–202.
18. Bregman-Reisler, H.; Doering, J. P. Optical Excitation in Collision of 500–5000 eV H_2^+, He^+, Ne^+, Ar^+, and N_2^+ Ions with CO_2. *J. Chem. Phys.* **1975,** *62*, 3109–3116.
19. Haugh, M. J.; Birely, J. H. Formation of Electronically Excited CO_2^+ in Collisions of H^+, H, He^+, and Ne^+ with CO_2. *J. Chem. Phys.* **1974,** *60*, 264–269.
20. Moore, J. H. The Excitation of near-UV Emission by H^+, H, and He^+ Impact on CO_2 and N_2O at 0.7–10keV. *J. Geophys. Res.* **1975,** *80*, 3727–3730.
21. Parker, J. E.; Milner, R. G.; Robertson, A. M. Energy Transfer and Primary Product Ion Excitation in He^+/CO_2 and H_2^+/CO_2 Charge-Transfer Collisions. *Int. J. Mass Spectrom. Ion Phys.* **1977,** *24*, 429–445.
22. Sim, W.; Haugh, M. Electronically Excited States of CO_2^+ Formed in Collisions of Heavy Ions with CO_2: Bending Vibrations Produced in the $A^2\Pi_u$ State of CO_2^+. *J. Chem. Phys.* **1976,** *65*, 1616–1623.
23. Holmes, J. L.; Mayer, P. M. Collison-Induced Photon Emissions from 8 keV $O_2^{+\cdot}$ and $CO_2^{+\cdot}$ Ion Beams. *J. Mass Spectrom.* **1995,** *30*, 52–56.
24. Burgers, P. C.; Holmes, J. L.; Szulejko, J. E.; Mommers, A. A.; Terlouw, J. K. The Gas Phase Ion Chemistry of the Acetyl Cation and Isomeric $[C_2H_3O]^+$ Ions. On the Structure of the $[C_2H_3O]^+$ Daughter Ions Generated from the Enol of Acetone Radical Cation. *Org. Mass Spectrom.* **1983,** *18*, 254–262.
25. Holmes, J. L.; Mommers, A. A.; Terlouw, J. K.; Hop, C. E. C. A. The Mass Spectrometry of Neutral Species Produced from Mass-Selected Ions by Collision and by Charge Exchange. Experiments with Tandem Collision Gas Cells. *Int. J. Mass Spectrom. Ion Processes* **1986,** *68*, 249–264.
26. Holmes, J. L. Assigning Structures to Ions in the Gas Phase. *Org. Mass Spectrom.* **1985,** *20*, 169–183.
27. Bloch, M.; Turner, D. W. Radiative Lifetimes of Ions Measured with the Photoelectron Spectrometer. *Chem. Phys. Lett.* **1975,** *30*, 344–346.
28. Maier, J. P.; Thommen, F. Fluorescence Quantum Yields and Cascade-Free Lifetimes of State Selected CO_2^+, COS^+, CS_2^+, and N_2O^+ Determined by Photoelectron-Photon Coincidence Spectroscopy. *Chem. Phys.* **1980,** *51*, 319–327.
29. Gauyacq, D.; Horani, M.; Leach, S.; Rostas, J. The Emission Spectrum of the CO_2^+ Ion: B to X Band System. *Can. J. Phys.* **1975,** *53*, 2040–2059.
30. Gauyacq, D.; Larcher, C.; Rostas, J. The Emission Spectrum of the CO_2^+ Ion: Rovibronic Analysis of the A to X Band System. *Can. J. Phys.* **1975,** *57*, 1634–1649.
31. Liu, J.; Chen, W.; Hsu, C.-W.; Hochlaf, M.; Evans, M.; Stimson, S.; Ng, C. Y. High Resolution Pulsed Field Ionization-Photoelectron Study of CO_2^+ ($X\ ^2\Pi_g$) in the Energy Range of 13.5–14.7 eV. *J. Chem. Phys.* **2000,** *112*, 10767–10777.
32. Liu, J.; Hochlaf, M.; Ng, C. Y. Pulsed Field Ionization-Photoelectron Bands for CO_2^+ ($A^2\Pi_u$ and $B^2\Sigma_u^+$) in the Energy Range 17.2–19.0 eV: An Experimental and Theoretical study. *J. Chem. Phys.* **2000,** *113*, 7988–7999.
33. Wang, L.-S.; Reutt, J. E.; Lee, Y. T.; Shirley, D. A. High Resolution UV Photoelectron Spectroscopy of CO_2^+, COS^+, and CS^+ Using Supersonic Molecular Beams. *J. Electron. Spectrosc. Relat. Phenom.* **1988,** *47*, 167–186.
34. McCallum, J. C.; Nicholls, R. W. Franck-Condon Factors and Related Quantities for the Fox-Duffendack-Barker (A to X) and Ultraviolet Doublet (B to X) Band Systems of CO_2^+. *J. Phys. B Atom. Mol. Phys.* **1971,** *4*, 1096–1101.
35. Herzberg, G. *Molecular Spectra and Molecular Structure I. Spectra of Diatomic Molecules*; Van Nostrand Reinhold: New York, 1950; p. 200.
36. Tokue, I.; Shimada, H.; Masuda, A.; Ito, Y.; Kume, H. Vibrational Distributions of the A $^2\Pi_u$ State of CO_2^+ and CS_2^+ Produced by Electron Impact on Jet-Cooled CO_2 and CS_2. *J. Chem. Phys.* **1990,** *93*, 4812–4817.
37. Atkins, P. Physical Chemistry, 6th Ed.; W. H. Freeman and Company: New York, 1998; p. 29.
38. Judge, D. L.; Bloom, G. S.; Morse, A. L. Studies of the CO_2^+ A to X Bands Using Photon Excitation from the Neutral Molecule. *Can. J. Phys.* **1969,** *47*, 489–497.
39. Wiese, W. L.; Smith, M. W.; Glennon, B. M. *Atomic Transition Probabilities*, Vol. I.; National Bureau of Standards: Washington, D.C., 1966.
40. Bashkin, S.; Stoner, J. O. Atomic Energy Levels and Grotrian Diagrams 1; North-Holland Publishing Company: New York, 1975.
41. Brundle, C. R.; Turner, D. W. Studies on the Photoionization of the Linear Triatomic Molecules: N_2O, COS, CS_2, and CO_2 Using High-Resolution Photoelectron Spectroscopy. *Int. J. Mass Spectrom. Ion Phys.* **1969,** *2*, 195–220.